Supplement of Geosci. Model Dev., 18, 10077–10094, 2025
https://doi.org/10.5194/gmd-18-10077-2025-supplement

Geoscientific Model Development
Open Access
EGU

Supplement of

Improvement of near-surface wind speed modeling through refined aerodynamic roughness length in high-roughness surface regions: implementation and validation in the Weather Research and Forecasting (WRF) model version 4.0

Jiamin Wang et al.

Correspondence to: Kun Yang (yangk@tsinghua.edu.cn)

S1. The settings of z_{0_Peng} in the WRF model

Before conducting the simulation of wind speed in the WRF model with the gridded z_{0_Peng}, we had adjusted the roughness length over vegetated fraction (z_{0_veg}) in each grid from z_{0_Peng}. Then, the default z_0 values in WRF over vegetated fraction were replaced with z_{0_veg}.

The mean shear stress ($\tau = \rho {u_*}^2$) in a grid is the sum of the shear stress over the bare and the vegetated areas weighted by vegetation fraction (*FVEG*):

$$ {u_{*mean}}^2 = {u_{*bare}}^2 * (1 - FVEG) + {u_{*veg}}^2 * FVEG \quad (1) $$

where u_{*mean} is the mean friction velocity (m/s) derived with z_{0_Peng}; u_{*veg} and u_{*bare} are the friction velocity in the vegetated and the bare fraction, which are derived with z_{0_veg} and the roughness length over the bare fraction (z_{0_bare}).

Under neutral conditions, z_{0_veg} can be expressed as:

$$ z_{0_veg} = e^{\ln(z_{ref}) - \left\{\left[\left(ln\left(\frac{z_{ref}}{z_{0peng}}\right)\right)^{-2} - (1-FVEG)*\left(ln\left(\frac{z_{ref}}{z_{0_bare}}\right)\right)^{-2}\right]*\frac{1}{FVEG}\right\}^{-\frac{1}{2}}} \quad (2) $$

where z_{ref} is the reference height (m), and z_{0_bare} and *FVEG* can be obtained from WRF model.

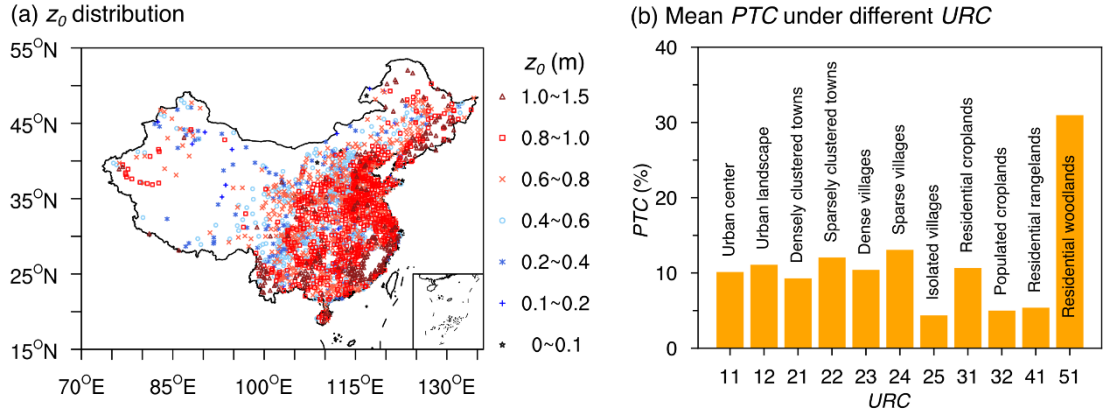

Figure S1. (a) Spatial distributions of annual mean $z_{0\_optimal}$ across 2,161 CMA stations. (b) Mean percent tree cover (*PTC*) for each *URC*. The numerical labels on the x-axis represent the *URC* codes, with the specific *URC* types annotated on the bars.

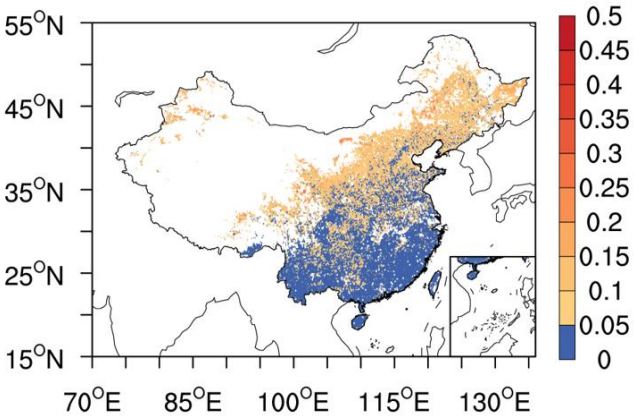

Figure S2. Spatial distributions of the standard deviation of monthly $\ln(z_{0\_RFR})$.

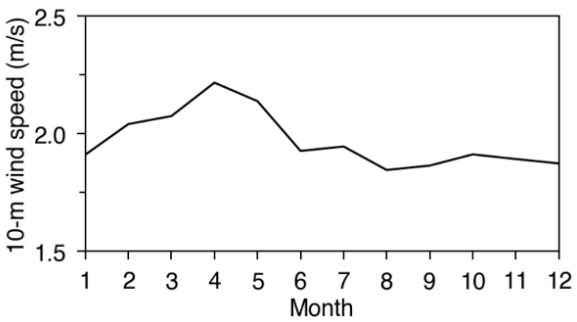

Figure S3. Monthly variations of the 10-m wind speed averaged over the d02 domain during 2015-2019 from ERA5.

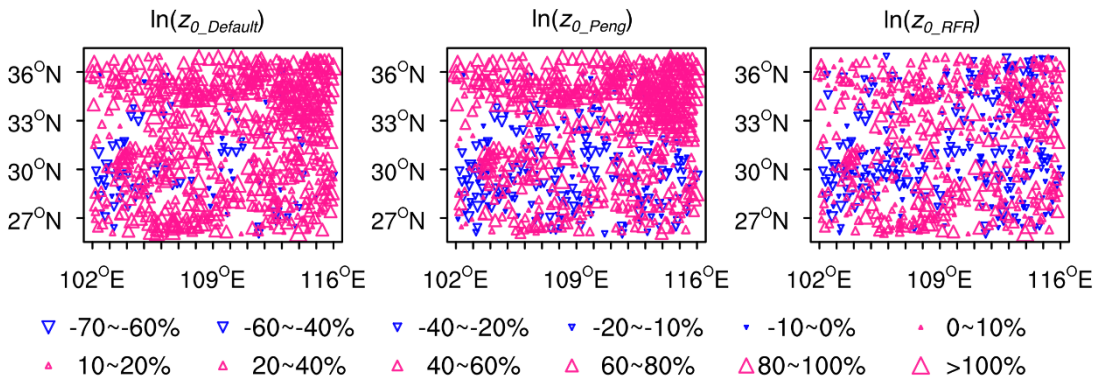

Figure S4. Distributions of mean bias percentage (*MBP*) in 10-m wind speed from simulations using $z_{0\_Default}$, z_{0_Peng} and z_{0_RFR} against observations from CMA stations.

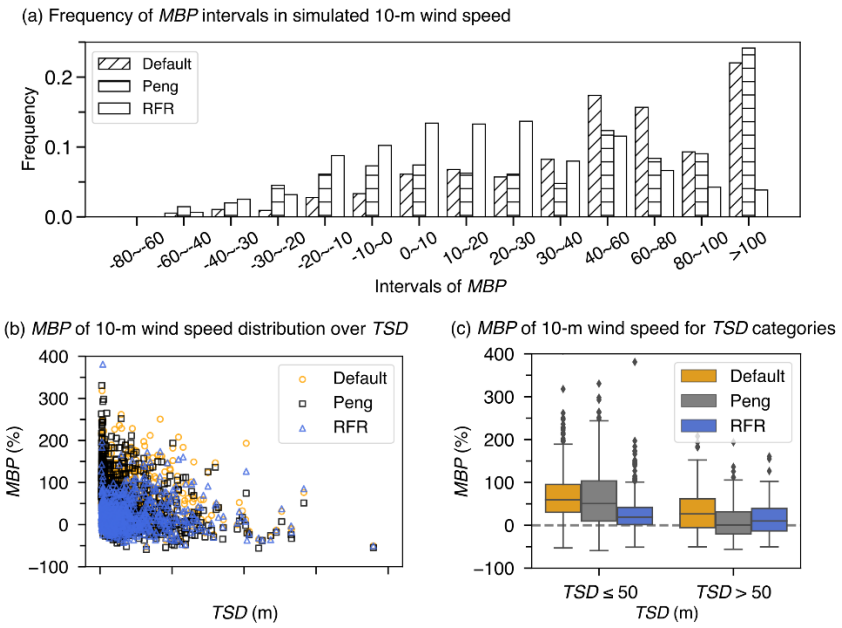

40 **Figure S5.** Same as Fig. 5 but for simulations in October 2019 instead of April.

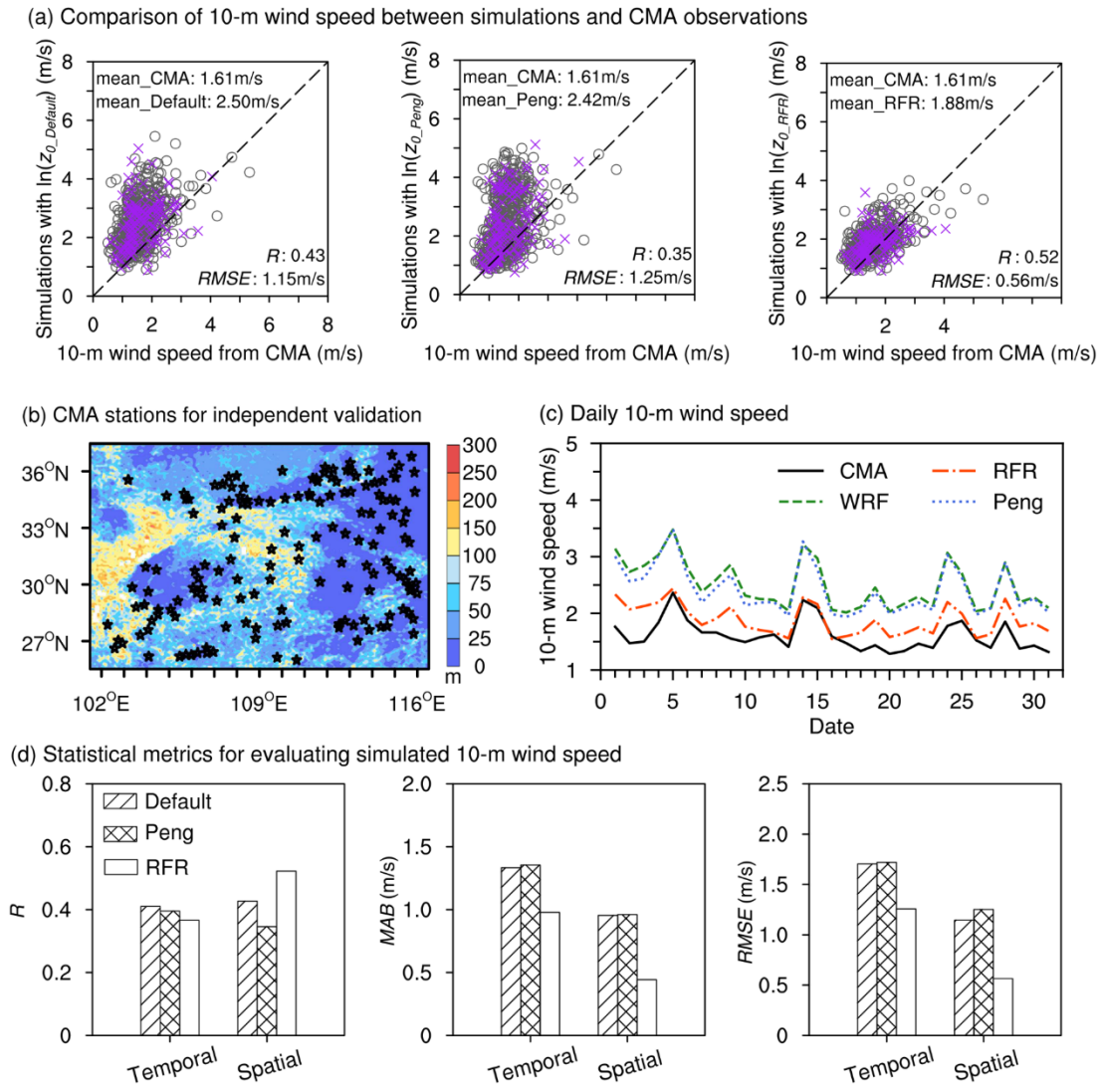

Figure S6. Same as Fig. 6 but for simulations in October 2019 instead of April.

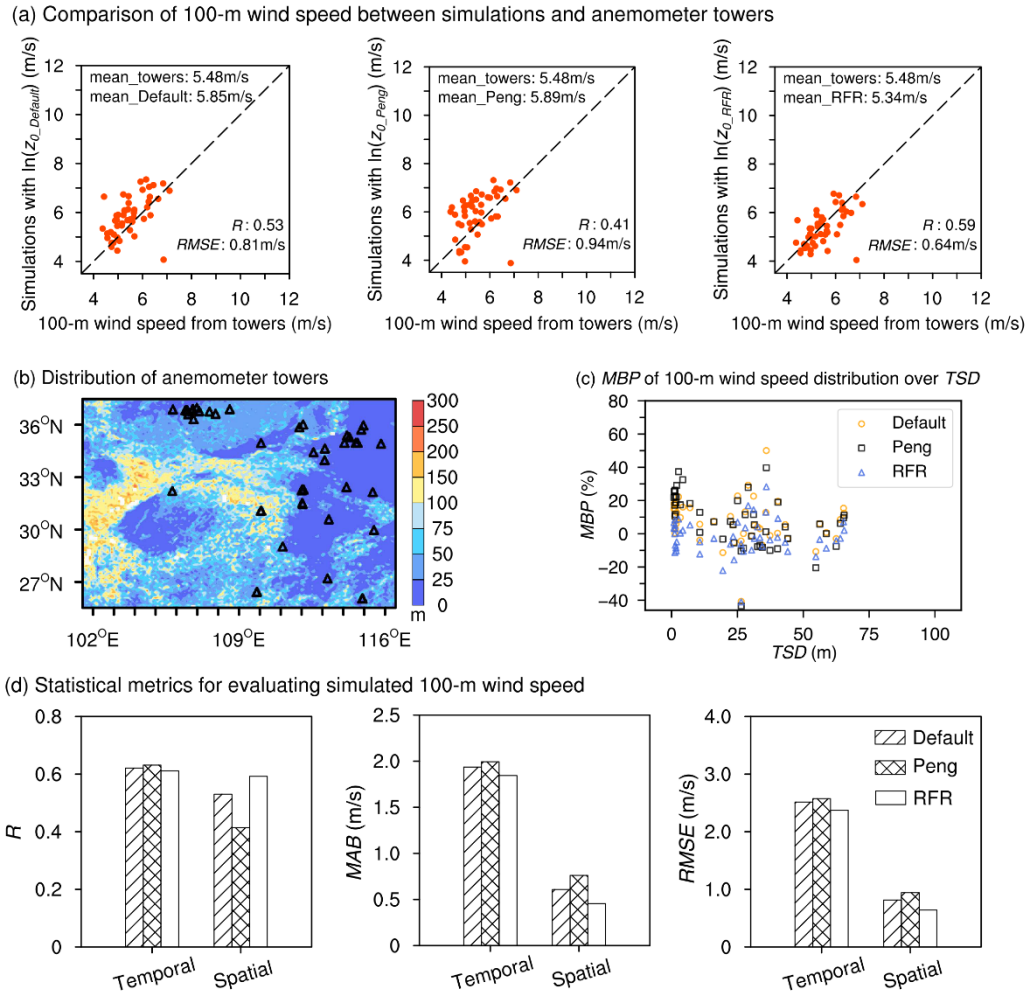

Figure S7. Same as Fig. 7 but for simulations in October 2019 instead of April. A total of 48 anemometer towers were used for 100-m wind speed evaluation.

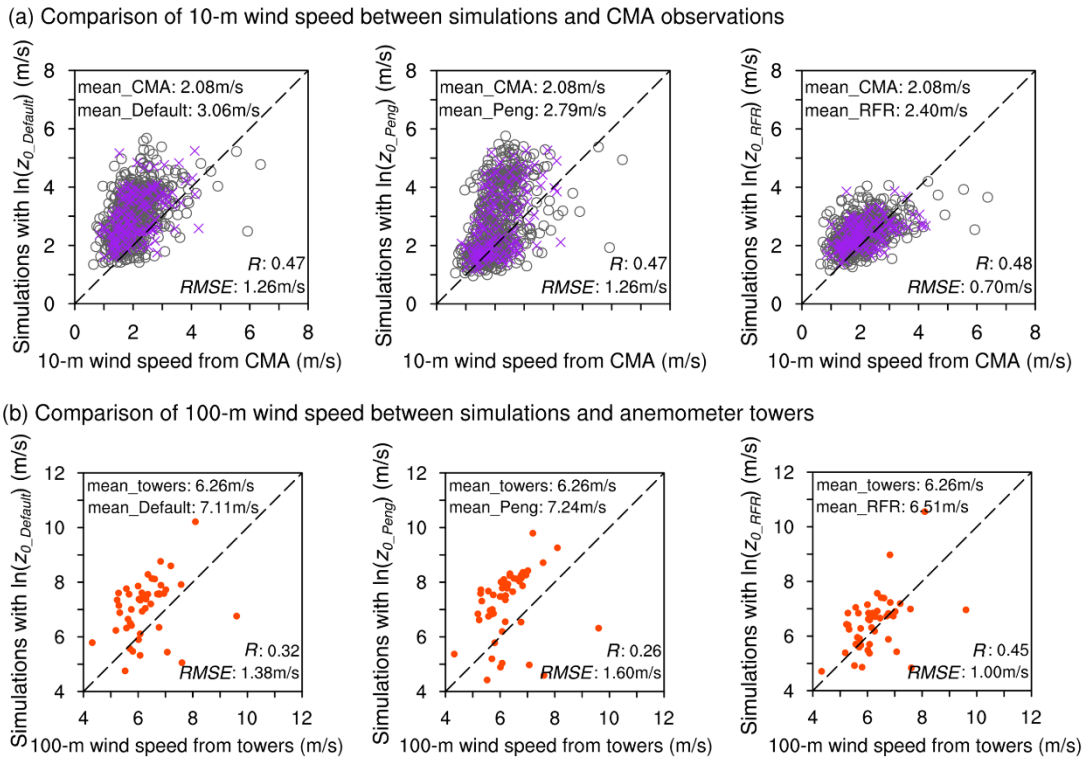

Figure S8. (a) Comparison of mean 10-m wind speeds in April between the coarse-resolution (0.09°; d01) simulations using $z_{0\_Default}$, z_{0_Peng}, and z_{0_RFR} and observations from CMA stations. All points (grey circles and purple crosses) represent the 753 CMA stations within the d02 domain available for comparison, while the purple crosses represent the 148 stations utilized for independent validation, which were not used in training the z_{0_RFR} model. (b) Comparison of mean 100-m wind speeds in April between the coarse-resolution (0.09°; d01) simulations using $z_{0\_Default}$, z_{0_Peng}, and z_{0_RFR} and observations from anemometer towers. The corresponding wind speed means, *R*, and *RMSE* of all stations are also indicated.

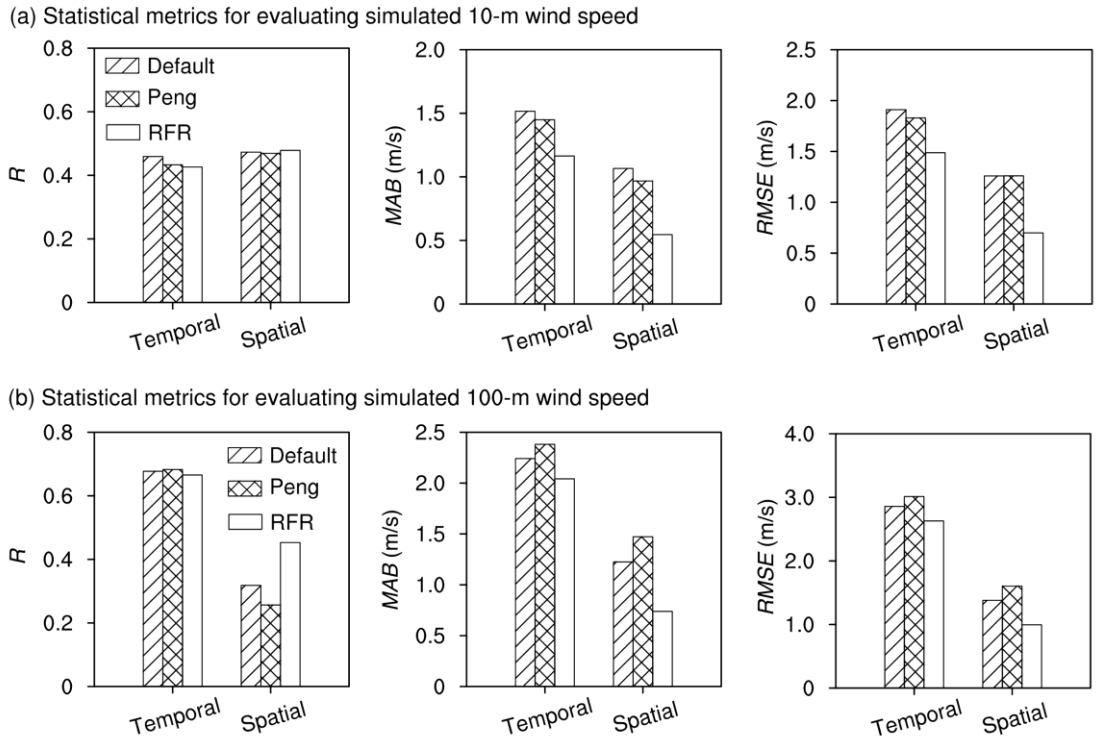

Figure S9. Statistical comparison of the coarse-resolution (0.09°; d01) simulations and observations within the d02 domain. (a) 10-m wind speeds from 753 CMA stations, and (b) 100-m wind speeds from 50 anemometer towers. Temporal and spatial *R*, *MAB*, and *RMSE* are included.

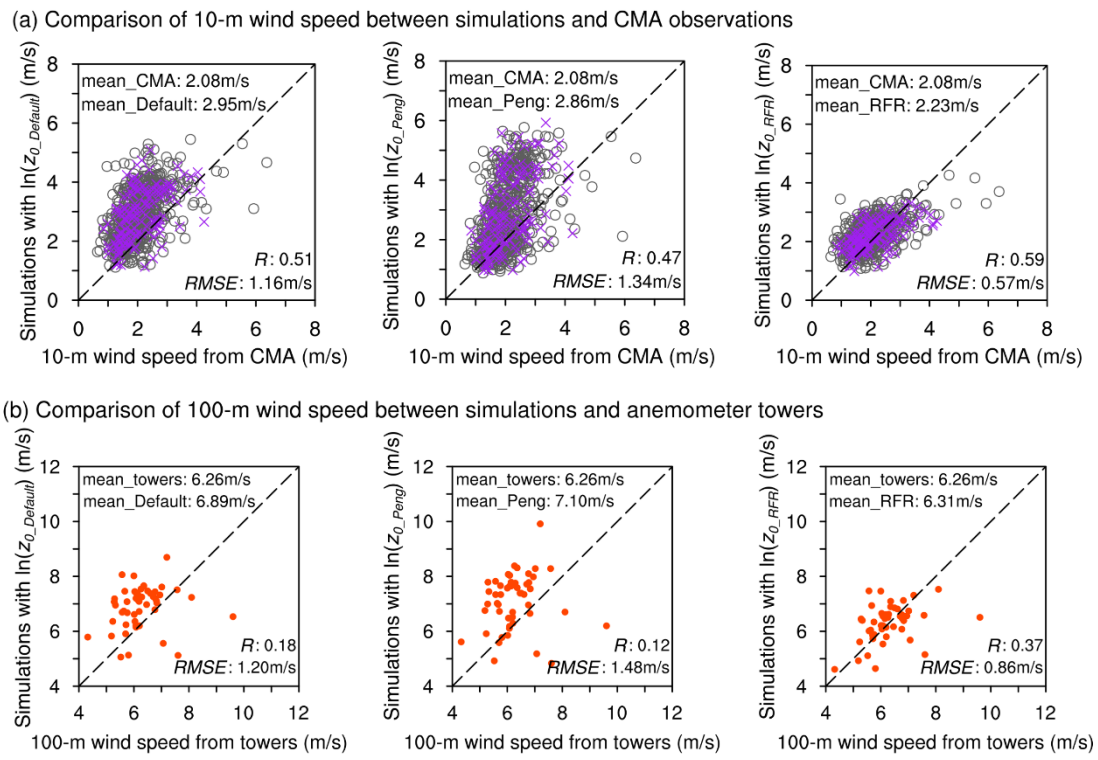

Figure S10. Comparison between simulated wind speeds and observations, with WRF driven by NCEP reanalysis data. (a) Comparisons of mean 10-m wind speed in April between the simulations using $z_{0\_Default}$, z_{0_Peng}, and z_{0_RFR} versus observations from CMA stations. All points (grey circles and purple crosses) represent the 753 CMA stations within the d02 domain available for comparison, while the purple crosses represent the 148 stations utilized for independent validation, which were from the test subset employed in z_{0_RFR} development. The corresponding wind speed means, *R*, and *RMSE* of all stations are indicated. (b) Comparisons of mean 100-m wind speed in April between the simulations using $z_{0\_Default}$, z_{0_Peng}, and z_{0_RFR} versus observations from anemometer towers. The corresponding wind speed means, *R*, and *RMSE* of all towers are also indicated.

Table S1. Mean 10-m wind speed at 753 CMA stations and mean 100-m wind speed at 50 anemometer towers from simulations and observations. Simulations were performed using $z_{0\_Default}$, z_{0_Peng}, and z_{0_RFR}, respectively, with NCEP reanalysis data used as the driving input for the WRF model. Also shown is the percentage reduction in wind speed error (*PRE*) achieved by z_{0_RFR} relative to $z_{0\_Default}$ and z_{0_Peng}.

	$z_{0\_Default}$	z_{0_Peng}	z_{0_RFR}	Observations
Mean 10-m wind speed (m/s)	2.95	2.86	2.23	2.08
PRE in 10-m wind speed (%)	82.8%	80.8%	-	-
Mean 100-m wind speed (m/s)	6.89	7.10	6.31	6.26
PRE in 100-m wind speed (%)	92.1%	94.0%	-	-

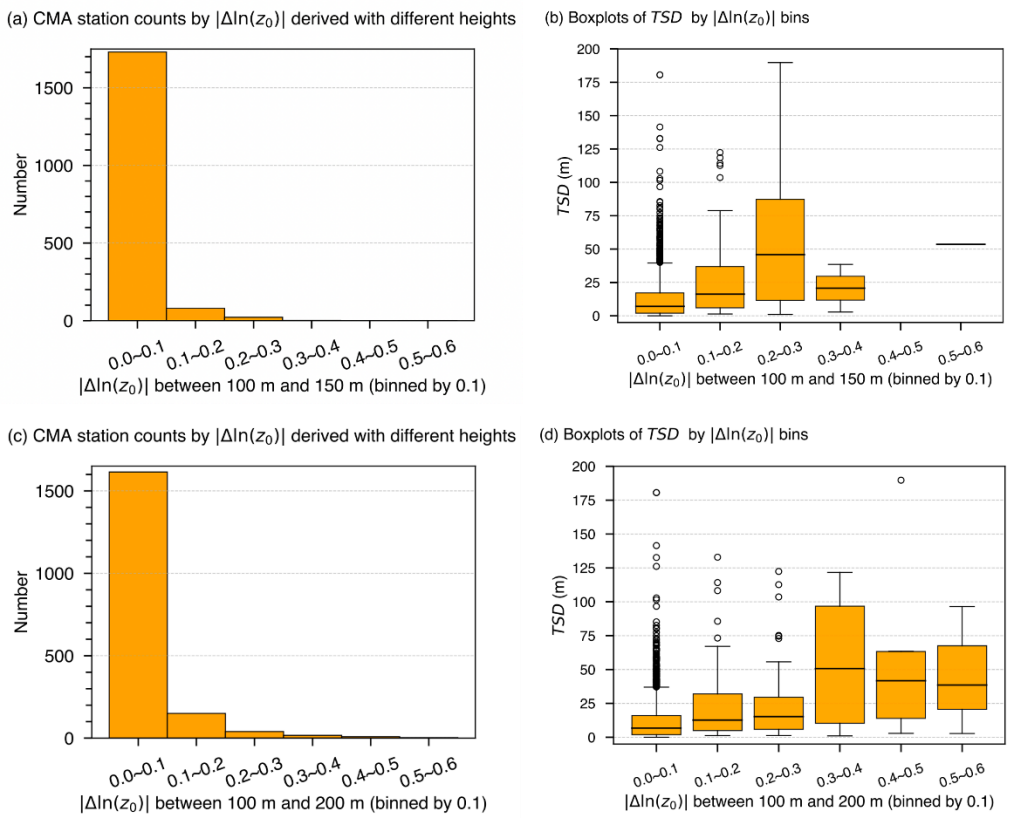

Figure S11. Sensitivity of the reference-height choice in Assumption 1 for z_{0_CMA} estimation. (a, c) Distributions of station counts by the absolute difference in annual-mean z_{0_CMA} values between estimates using 150 m (a) or 200 m (c) and those using 100 m. (b, d) Boxplots of *TSD* across bins of the absolute difference in annual-mean derived $ln(z_0)$. (b, d) Boxplots of *TSD* versus binned absolute differences in annual-mean z_{0_CMA}, computed relative to the 100-m–based estimate for 150 m (b) and 200 m (d).